

This document is the Accepted Manuscript version of a Published Work that appeared in final form in ACS Sensors, copyright © American Chemical Society after peer review and technical editing by the publisher. To access the final edited and published work see <https://doi.org/10.1021/acssensors.2c01827>

Access to this work was provided by the University of Maryland, Baltimore County (UMBC) ScholarWorks@UMBC digital repository on the Maryland Shared Open Access (MD-SOAR) platform.

Please provide feedback

Please support the ScholarWorks@UMBC repository by emailing scholarworks-group@umbc.edu and telling us what having access to this work means to you and why it's important to you. Thank you.

A step forward for smart clothes—fabric-based microfluidic sensors for wearable health monitoring

Tao Zhang¹, Adam Michael Ratajczak¹, Hui Chen², John A. Terrell¹, and Chengpeng Chen^{1,*}

1. Department of Chemistry and Biochemistry,
University of Maryland Baltimore County,
MD, USA, 21250
2. Department of Chemical, Biochemical and Environmental Engineering,
University of Maryland Baltimore County,
MD, USA, 21250

*Corresponding to: Dr. Chengpeng Chen
1000 Hilltop Circle, Baltimore, MD, USA
Chemistry and Biochemistry
University of Maryland Baltimore County
+1-4104553053
cpchen@umbc.edu

ABSTRACT

We report the first demonstration of fabric-based microfluidics for wearable sensing. A new technology to develop microfluidics on fabrics, as a part of undergarment, is described here. Compared to conventional microfluidics from polydimethylsiloxane, fabric-based microfluidics are simple to make, robust, and suitable for efficient sweat delivery. Specifically, acrylonitrile butadiene styrene (ABS) films with precut microfluidic patterns were infused through fabrics to form hydrophobic areas in a specially controlled sandwich structure. Experimental tests and simulations confirmed the sweat delivery efficiency of the microfluidics. Electrodes were screen-printed onto the fabric-based microfluidic. A novel wearable potentiometer based on Arduino was also developed as the transducer and signal readouts, which was low-cost, standardized, open-source, and capable of wireless data transfer. We applied the sensor system standalone or as a module of a T-shirt to quantify $[Ca^{2+}]$ in a wearer's sweat, with physiological and accurate results generated. Overall, this work represents a critical step in turning regular undergarments into biochemically smart platforms for health monitoring, which will broadly benefit human healthcare.

Keywords: wearable sensor, microfluidics, potentiometry, Arduino, smart clothes

Wearable biochemical sensing is significant because of its capability for continuous health monitoring in a real-time and non-invasive manner.¹⁻⁴ There are various biofluids that can be targeted for biomarker screening⁵⁻⁷, including blood, tears, urine, and saliva.⁸⁻¹⁰ Nonetheless, blood is difficult to access for non-invasive and continuous detections; the on-and-off nature of tears is not suitable for immediate real-time monitoring, and nor is urine; while saliva is continuously produced, it can be dramatically affected by food or drinks. Therefore, sweat has recently gained great attention and interest in both academic and industrial research, as an ideal biofluid for continuous health monitoring.¹¹⁻¹⁵ Sweat is secreted continuously on body surface—around 3 $\mu\text{L}/\text{min}$ with inaction and over 10 $\mu\text{L}/\text{min}$ when sporting for adults per square centimeter.^{16, 17} Moreover, sweat contains a rich library of chemicals, such as metabolites, proteins, hormones, and ions, which can provide extensive physiological insights.¹⁸⁻²⁰ The concentrations of the chemicals in sweat are also found correlated with their blood levels.²¹

Since 2016, when Roger's group first reported a wearable colorimetric microfluidic sensor²², various wearable sensor platforms have been reported, which can be generally categorized into two groups: static and microfluidic. Static sensors apply a substrate as an exposed detection area directly attached onto human skin to measure the target analytes.²³ A typical example is a flexible polyethylene terephthalate patch with screen-printed electrodes, which can be taped or fastened on skin for biochemical analyses in sweat.²³⁻²⁵ Although the setup is simple and straightforward, sample turnover can be a notable problem—accumulated molecules from sweat at the detection area may not be refreshed efficiently, compromising the temporal resolution for effective continuous measurements. Microfluidic models, on the other hand, apply fluidic features for active sweat delivery through the detection zone (e.g., electrochemistry or colorimetry) via nature pressure (~ 70 kPa) produced from the dermal duct of the sweating pores and capillary forces.²⁶

Currently, most reported microfluidic wearable sensor platforms are made from soft lithography based on polydimethylsiloxane (PDMS).²⁷⁻³⁰ Nonetheless, such devices require well-trained personnel and extensive facilities to be fabricated, applied, and maintained, which can prevent broad adoption of the technology from technical, costly, and applicable perspectives. New microfluidic platforms that are simple to produce, robust, comfortably wearable, allowing detector integration, and can effectively deliver sweat will be critical for wearable biochemical sensing applications.

There is a technology that might work for the purpose — paper-based 2D microfluidics, which utilizes capillary actions to drive liquid flow within channels defined by hydrophobic barriers.³¹⁻³⁶ Due to its simplicity, wax printing has been the prevailing method to create hydrophobic barriers through paper substrates.³⁷⁻³⁹ However, it is challenging to apply a paper-based microfluidic for sweat analyses on human body surfaces because paper loses its integrity after being soaked.

Nonetheless, because both paper and fabrics are 2D materials with some shared physical properties, paper-based microfluidics highly inspired us for the presented work—could we directly make microfluidic on undergarments? People wear such clothes mainly for sweat absorbing anyway, and having well-defined microfluidics on them for orderly sweat delivery through the integrated analytical scheme would be an ideal way for continuous biochemical assessment of a wearer's health. Take cotton, a common fabric for undergarments, for example, the fabric remains integrity when being soaked in sweat and can drive liquid flow via capillary actions.⁴⁰

Creating the hydrophobic barriers through fabrics to define microfluidic channels and reservoirs is critical. A few papers have shown successful wax-printing of microfluidics on fabrics^{39, 41}. However, the applications were not different from paper-based apparatus (just switching paper by fabrics for similar applications).^{42, 43} The suitability of such apparatus for wearable sensing has not been tested. While proprietary, the wax used to print paper-based microfluidics is mainly paraffin-based.⁴⁴ It is challenging to wax-print microfluidics on a wearable device because paraffin starts to soften and melt above 35 °C⁴⁵ (human surface temperature is typically higher than this⁴⁶), causing ever-changing microfluidic structures and uncomfortable wearing experiences (due to the melted wax). As shown in **Fig. S1** in the supplementary information (SI), a microchannel printed by paraffin in cotton fabrics was dramatically deformed after being incubated at 37 °C. Similar phenomena were observed with channels printed from another common wax, soy wax. Soft lithography is another way to make paper-based microfluidics by infusing photopolymers (e.g., SU-8) through a substrate, followed by photomasking to cure the polymer in the predesigned hydrophobic areas.⁴⁷⁻⁴⁹ However, this method takes many steps and utilizes a large amount of organic solvents (so that liquid waste; e.g., dimethylformamide and isopropyl alcohol).⁵⁰ Therefore, we developed a new technology using acrylonitrile butadiene styrene (ABS) film printing to create hydrophobic barriers through fabrics for robust and precise microfluidic development. our technology is highly reproducible for precisely controlled

microchannels and reservoirs, with the capability of detector integration. Also, the simplicity and scalability of the technology makes it potentially translational to broadly benefit wearable sensor developments.

We tested the sensor platform via measuring Ca^{2+} contents in sweat in a wearable format. The sensor was worn standalone or as a module of a T-shirt. A biochemical sensor must be connected to electronic transducers and displays for data readouts. While exciting but complex integrated microelectronic circuits have been reported by several groups^{23, 51}, here, we creatively developed an Arduino based (4 cm x 1.5 cm x 0.3 cm) wearable potentiometric transducer for data processing and wireless transfer. Due to the low-cost, standardization, and small size of the Arduino board, its marriage with the fabric-based microfluidic platform will potentially enhance the wide application of wearable sensors to promote human healthcare. We thoroughly tested the sensor on human skin and validated the results via ion chromatography, which showed high accuracy and reproducibility. Overall, this work is a critical step forward toward smart clothes with health readouts from e.g., T-shirts and pajamas, which represents high novelty and significance.

Experimental

Chemicals and Materials

Magnesium chloride (MgCl_2), polyvinyl chloride (PVC), bis(2-ethylhexyl) sebacate (DOS), sodium tetrphenylborate, calcium ionophore II, and tetrahydrofuran (THF) were purchased from Millipore-Sigma (MO, US). Hydrochloric acid (HCl), potassium chloride (KCl), and acetone were purchased from Thermo Fisher Scientific (MA, US). Sodium chloride (NaCl) and calcium chloride (CaCl_2) were purchased from Alfa Aesar (MA, US). Silver/silver chloride (Ag/AgCl) and carbon inks were purchased from Ercon Inc. (MA, US). Acrylonitrile butadiene styrene (ABS) and polystyrene were purchased from McMaster-Carr (IL, US). Microfluidic syringe pumps were obtained from New Era (NJ, US). Artificial sweat was purchased from Nano Chemazone (Canada). Cotton fabric and white cotton t-shirts were purchased from Walmart (Ar, US, thickness= 0.3 mm).

Development of fabric-based microfluidics with ABS film printing

As shown in **Fig. S3** in the supplementary information, an ABS film (thickness = 0.08 mm) was laser cut (raster power 100%, vector current 18%) to form the shape of the hydrophobic areas of the planned microfluidic device. Next, the ABS pattern was placed on top of a piece of cotton fabric. The ABS-fabric stack was then placed on top of a layer of paper towel soaked with acetone.

The amount of acetone in the paper towel was a key parameter for successful microfluidic fabrication—the acetone needed to just dampen the paper towel without dried areas or dripping liquid. For the paper towel we used, 3 mL acetone was added to a square feet of paper towel. The acetone from the paper towel diffused up through the fabric layer to dissolve the ABS pattern atop. And the dissolved ABS then diffused down into the fabric to form the hydrophobic areas. The treatment time was critical, as we found too long treatment would cause lateral smearing of the ABS compromising the microfluidic structure. We tested various fabrication times between 1 to 60 s to determine the optimal.

Microfluidics of various structures were designed throughout the whole study. The single reservoir-channel design (**Fig. 1B**) was used to characterize the integrality of microfluidics under different acetone treatment times, the correction of the width of the channel between CAD design and, on fabric, and the simulations. The design with two reservoirs (**Fig. 4A**) was used to characterize flow rates and efficiency. The design with three reservoirs and a joint channel (**Fig. 5A**) was applied as the wearable microfluidic for sweat analyses. The three reservoirs were designed for the integration of two working electrodes and one reference electrode, respectively.

Dimension characterization of the fabric-based microfluidics

Because the fabrication process involved acetone dissolving, the final channel size might differ from the size in the ABS pattern. To test if this was true, and if so, was there a correlation between the two dimensions, we measured the channel sizes in the ABS patterns and the final microfluidic devices on the fabrics. The channel width in an ABS pattern formed by a laser cutter was measured by a caliper. A channel was measured five times at random locations for one imaging. The channel width of the resulting fabric-based microfluidic device was measured under a calibrated optical microscope after adding a blue dye solution to the microfluidic for sharper color contrasts.

Drainage test of the fabric-based microfluidics

A holder was 3D printed with a Fused Deposition Modeling (FDM) 3D printer and combined with Tygon tubing (inner diameter = 1.5 mm). A reservoir on the fabric-based microfluidics was robustly attached to the tubing outlet of the holder without gaps using double-sided tape. A syringe pump with a needle (Gauge 16) was connected to the tube. A water-based dye solution (10 μ L) was added to a reservoir before the flow experiments. Then pure water from the syringe pump at different rates was delivered to the reservoir to wash out the dye at

physiological sweating rates under various situations (inaction vs. sports), including 3, 5, and 10 $\mu\text{l}/\text{min}$. An aliquot of 2 μl solution was taken using a pipette from the reservoir area at different time points (**Fig. 4D**). The sample was then mixed with 200 μl DDI (doubly de-ionized) water in a 96-well plate. The absorbance at 630 nm of the diluted samples was measured by a plate reader (SpectraMax i3x, Molecular Devices). The initial pigment solution was defined as 100% concentrated, and a calibration curve was premade with dilutions of the initial solution. The percentage of the dye remaining in the reservoir area at different times was then calculated.

The shape of the reservoirs was optimized via COMSOL simulations with the most efficient sweat delivery. In COMSOL, cellulose was chosen as the substrate material with fluid speed scanning from 1 to 3 mm/min to mimic sweat passing the fabric layer. Also, a reservoir was designated as an inlet and the end of the merging channel was designated as the outlet.

Electrode integration on the fabric-based microfluidics

As shown in **Fig. 5B**, three electrodes were screen printed onto the three reservoirs of the microfluidic device. The two electrodes in the side reservoirs were working electrodes (duplicates) while the one in the middle served as the reference electrode. A printing stencil was designed in CorelDraw and laser cut from a polyester film (thickness = 0.25 mm). Ag/AgCl printing ink was spread onto the stencil with a squeegee to screen-print electrodes onto the three reservoirs of the fabric microfluidics. The electrodes were 1 mm by 5 mm rectangles. After the Ag/AgCl ink was dried under 37 °C for 24 h, the carbon ink was screen printed onto the Ag/AgCl layer in the two side reservoirs as the electron transducing layer, followed by drying at room temperature overnight. To make a Ca^{2+} selective electrode, a Ca^{2+} membrane cocktail was made containing 1% Ca^{2+} ionophore II, 64.5% DOS, 33% polyvinyl chloride, 0.5% sodium tetraphenylborate in THF (all concentrations in w/w). An aliquot of 5 μl of the membrane cocktail was then dropped onto the indicator electrodes. Next, the electrodes were left in a fume hood for 12 hours for the THF to dry out completely. The reference electrode was coated with a mixture made of polyvinyl butyral (PVB) saturated with NaCl. This mixture was made by dissolving 50 mg of NaCl and 79.1 mg PVB in 1 mL methanol. An aliquot of 3 μl of the PVB mixture was dropped onto the reference electrode, followed by air drying for 2 hours, to provide constant $[\text{Cl}^-]$ around the reference electrode, and thus stable potential. The leads of the electrodes were connected to copper wires (diameter= 0.5 mm) via soldering.

The Arduino program and setup

The program was written in the free Arduino IDE software. Arduino Nano 33 board was applied as a connected part to a computer or a wearable device. The board in the wearable device could receive all initial data input from the fabric-based microfluidic sensor, process the data, and send the data wirelessly via low-energy Bluetooth to devices such as a smart phone. The App of Phyphox was used to receive the data on an Android phone. All programs are included in the SI.

Characterization of the analytical merits of the wearable sensor

General setup. Because the physiological concentration of Ca^{2+} in sweat is between 0.2 mM and 2 mM^{52, 53}, five Ca^{2+} standards were prepared in Ca-free artificial sweat at 0.125 mM, 0.25 mM, 0.5 mM, 1 mM, and 2 mM. The microfluidic wearable sensor with Ca^{2+} selective electrodes was connected to an Arduino Nano 33 board via A0 and A6 (indicator electrodes) and GND port (reference electrode). Each standard solution was flown into the microfluidic reservoir at 3 $\mu\text{l}/\text{min}$ for 40 s, starting from 0.125 mM to 2 mM. The voltage was read by Arduino per second. The voltage readings from each standard solution were averaged and then plotted against the negative log of Ca^{2+} concentration (pCa) to generate a calibration curve.

Selectivity characterization. The possible interfering ions in sweat were tested in relevant/excessive amounts to determine the selectivity of the sensor for Ca^{2+} . Five mixtures in water were prepared: 1 mM CaCl_2 , 1 mM CaCl_2 + 3 mM HCl, 1 mM CaCl_2 + 5 mM KCl, 1 mM CaCl_2 + 10 mM NaCl, 1 mM CaCl_2 + 0.25 mM MgCl_2 (the physiological concentrations of H^+ , K^+ , Na^+ , and Mg^{2+} in sweat are around 3 mM, 1 mM, 10 mM, and 0.1 mM, respectively²⁶). Each solution was flown to the reservoir at 3 $\mu\text{l}/\text{min}$ for 30 s and then switched to the next one with autonomous readings by the programmed Arduino every 1 s.

Accuracy characterization. A. M. Ratajczak made two standard Ca^{2+} solutions in calcium-free artificial sweat (0.5 mM and 1.0 mM) and gave them to T. Zhang for analytical recovery without telling him the concentrations (blind). A calibration curve was obtained by T. Zhang as described above, which was used to calculate the concentrations of the “unknowns”. The tested and true values were then compared.

Reproducibility characterization. The measurements above (calibration curve, selectivity tests, and unknown recovery) were conducted on >10 devices fabricated from different batches on different days. All data were compared and pooled together so that error bars could tell the reproducibility.

Near real-time Ca^{2+} sensing on the human surface

Standalone measurement. A fabric-based microfluidic sensor was attached to the arm of a human via surgical tape. The Arduino nano board was connected to the microfluidic device through soldered wires for voltage reading and transducing in near real-time (5 s per measurement). The board was fastened on the wearer's arm by a sports loop band. We monitored Ca^{2+} in sweat for 25 min. Sweat around the sensor area was sampled by a pipette (10 μL) every 6 min for ion chromatography measurements of Ca^{2+} , as validations of our sensor results.

Worn as a part of a T-shirt. The sleeve part of a T-shirt was laser cut to form a square hole of the same size as the fabric-based microfluidic device. The sensor was placed in the hole with the edges joined by narrow tape strips. A similar Arduino board described above was applied, but with the program to wirelessly send processed data to a phone in near real-time (**Fig. S6** in the SI). The same sampling method was taken to collect sweat in the sensor area for result validation.

Ion-chromatography measurements of Ca^{2+} in the collected sweat

The Ca^{2+} content in sweat was measured via ion chromatography with a Thermo Scientific Dionex Integrion instrument. Ca^{2+} was separated along an IonPac CS16 column using reagent-free ion chromatography with a water mobile phase consisting of 30 mM sulfuric acid. Due to the low sample volume, 10 μL of each sweat sample was spiked into 5 mL standard Ca^{2+} solutions (0.5 mM) and submitted for IC measurement. Then, the Ca^{2+} content in sweat was calculated from the difference of the before- and after-spike standards. **Fig. S7** shows an example chromatograph of standard 0.5 mM Ca^{2+} with and without the 10 μL sweat sample. The calibration range for this measurement was 0 to 1.25 mM (the five standards were 0.25 mM, 0.5 mM, 0.75 mM, 1 mM, and 1.25 mM) and the regression coefficients of determination (R^2) were greater than 0.99.

Data analysis and statistics

The t-test and ANOVA were applied to compare data groups, and a significant difference was confirmed only when p values were smaller than 0.05.

Result and Discussion

The novel fabric-based microfluidics

To develop microfluidics on fabrics for sweat delivery, the hydrophobic areas that will define fluidic channels and reservoirs will be the critical step. Paraffin wax, although commonly used to make paper-based microfluidics, cannot be used for this purpose due to the high meltability at body surface temperature. While photoresists might be applicable, the process is tedious with large amounts of organic wastes (solvents) produced. When we were searching for suitable hydrophobic

polymeric materials to develop fabric-based microfluidics, acrylonitrile butadiene styrene (ABS) caught our attention because this plastic is inexpensive and low allergenic. More importantly, ABS dissolves in common solvents, such as acetone, and thus can be easily manipulated to diffuse through a porous substrate (e.g., fabrics) to form hydrophobic blocking areas. We initially tested swabbing on fabrics with dissolved ABS in acetone. Although the ABS could infiltrate through the fabrics, the microchannels made thereby were irreproducible in terms of the overall size and size variations of the same channel. Having a uniform layer of patterned ABS, like an ABS film, on top of a piece of fabric, with well-controlled infiltration, would likely produce precise and reproducible microfluidic structures. Although hot-pressing/lamination is widely used to combine ABS films onto a substrate, we found that this method is not sufficient to full melt the ABS, neither infiltrate the ABS into the fabrics. (**Fig. S2** in the SI). Therefore, we developed a new technology using flexible ABS films assisted with acetone in a sandwich. As illustrated in **Fig. 1A**, a microfluidic pattern was formed on an ABS film via laser cutting, with the void parts being channels and reservoirs in the resulting fabric microfluidics. This ABS pattern was placed on a piece of cotton fabric sitting on paper towel saturated with acetone. At room temperature, acetone liquid and its vapor could diffuse up through the cotton fabric layer to dissolve the ABS on top, which would then diffuse down through the fabric to form hydrophobic areas. **Fig. 1B** shows a simple reservoir-channel microfluidic device fabricated thereby to show the method's performance. **Fig. 1B (i)** was the microfluidic pattern cut from an ABS film. As can be seen in **Fig. 1B (ii)** and **(iii)**, the front (where ABS was laid onto) and back sides of the fabric microfluidic device, respectively, the dissolved ABS (the darker area) completely infiltrated through the fabric layer after 10 s. The unaffected parts (the lighter area) were still cotton fabric and thus hydrophilic. After pipetting a blue food dye solution into the circular reservoir, the liquid could flow out of the channel without leakage out of the hydrophilic areas as shown in **Fig. 1B (iv)**.

The treatment time by the acetone vapor within the sandwich was critical. Insufficient ABS dissolving and/or infiltration would not form a tight hydrophobic seal through the fabric. On the other hand, too much time would cause an overflow of the dissolved ABS laterally, compromising the channel and reservoirs (e.g., causing shrunk channels). Therefore, we tested the treatment times between 0 and 60 s using the microfluidic model in **Fig. 1B**. After adding the blue dye solution to the reservoir and letting it flow out of the channel, we measured the blue area (A_b) in ImageJ. The designed area of the channel and reservoir was A_d (measured from the pre-cut ABS pattern). We

defined the term “leakage percentage” via **Equation 1** below. If the blue area was larger than the designed area, or a leakage percentage higher than 0, it meant the solution leaked out of the reservoir/channel. If the blue area was smaller than the designed area, with the leakage percentage being negative, it suggested ABS lateral diffusion shrinking the hydrophilic areas.

$$\text{Leakage percentage} = \frac{(A_b - A_d)}{A_d} \times 100\% \quad \text{Equation 1}$$

As shown in **Fig. 1C**, with a treatment shorter than 5 s, significant leakage was observed. Between 5 and 20 s, a leakage percentage of 0 was achieved, indicating perfect infusion of the ABS. When the treatment was longer than 20 s, the leakage percentage started to be negative values, indicating undesired lateral ABS smearing. **Fig. 1D** further supported these observations based on channel width measurements of the resulting fabric-based microfluidics. Also, with too long treatment, the width variance of the same channel drastically increased (**Fig. 1E**). Based on these findings, we determined the optimal treatment time of 10 s for our research.

We used ABS film of 0.08 mm thick, the thinnest we could find commercially available. The cotton fabric was directly cut from a regular white T-shirt (0.3 mm thick), which was sufficient for our purpose of clothes-based wearable sensing. However, if fabrics and ABS films of other physical properties will be used, we anticipate different optimal treatment time may apply, which can be determined by similar methods presented here.

Characterization and optimization of the microfluidic feature

Because ABS is a thermal plastic, the cutting edges by a laser might melt more than expected. Therefore, we first compared the channel width designed in CAD, and the resulting channel width after cutting the CAD design through the ABS film. As shown in **Fig. 2A**, the blue dots are the designed channel widths in CAD (400, 500, 600, 700, 800 μm , respectively) and the grey ones are the channel widths in the cut ABS patterns. The widths were significantly higher than the designs, likely caused by the over-melting of the ABS along the cutting traces. Nonetheless, this size change was reproducible and calibratable. The actual size on the ABS film was $\sim 200 \mu\text{m}$ larger than the design for all the widths tested. The channel size in the ABS pattern was nearly the same as the channel width on fabric after the ABS film printing for 10 s, as shown in the orange dots/line. **Figs. 2B** shows the bright field microscopic views of the channels filled with the blue dye solution,

without leakage observed. We also incubated the fabric-based microfluidics at 37 °C for 72 hours and did not see ABS melting or smearing that could compromise the microfluidic structures (**Fig. 2C**), which validated the long-term wearability of the platform. Because our laser-cutter cannot process cuttings smaller than 400 μm through ABS, also considering the 200 μm enlargement of a cut pattern than its CAD design, channels of 600 μm was the smallest that could be achieved.

Optimize the channel size and reservoir shapes

A key reason to include microfluidic features on the wearable sensor is for efficient sweat delivery and thus sample refreshing in the detection zone. Human sweat glands are comprised of a secretory coil where sweat is initially produced and a dermal duct that pumps sweat via the epidermis to the surface with a natural pressure of ~ 70 kPa.²⁶ With the microfluidic reservoirs collecting sweat pumped out of the glands, the microfluidic channel could facilitate directional delivery of sweat via capillary actions. With a smaller channel, the capillary action force is larger, but the flow flux is smaller, and vice versa. Hence, we experimentally compared the liquid delivery efficiency of various channel widths on the fabric. As shown in **Fig. 3A**, with increased widths from 600 to 800 μm , the volumetric flow rate was faster (shortener drainage time), and after 800 μm , the flow rates were not affected by the channel width anymore (channel length = 2.5 mm). The channel width of 800 μm was determined the optimal then, and used in subsequent studies.

To find the most suitable reservoir shape, the COMSOL Multiphysics, one of the most powerful computer simulation software⁵⁴, was used to simulate the fluids in the fabric-based microfluidic. As seen in **Fig. 3B**, the velocity field (dark blue to red=lowest to highest velocity) in the different reservoir shapes with the same channel widths (800 μm) were simulated. Flow-stagnancy areas in a microfluidic reservoir, especially for wearable sensor detection, would ideally be as small as possible, providing efficient washing and thus accurate results for continuous near real-time detections. **Fig. 3B** indicates the velocity fields in the reservoir shapes, including rectangular, triangle, circular, rhombus, and oval. The ratio of areas with the lowest velocities ($<15\%$ of the gross average) was calculated in the various shapes. (**Fig. 3C**) The oval (long axis parallel to the channel) showed the least low-velocity areas and thus the most homogeneity, which was thus determined as the optimal reservoir shape for subsequent applications.

Sweat delivery efficiency validation

Based on the optimization above, we fabricated fabric-based microfluidic devices shown in **Fig. 4A** (front and back views) with oval reservoirs and 800 μm wide channels. Also, SEM images of this microfluidic device were shown in **Fig. 4B** (top = joint outlet channel, bottom = individual channel for a reservoir). Water-based blue dye solution (10 μL) was pipetted onto the reservoir and followed by air drying. As shown in **Fig. 4C**, we 3D-printed a holder where the microfluidic device could be taped onto. The holder contained a tubing connected to a syringe, with the outlet touching a reservoir of the microfluidic device. The dye-saturated reservoir was then washed with artificial sweat at 3, 5, and 10 $\mu\text{L}/\text{min}$, respectively. These flow rates reflected physiological sweating rates^{16, 17}. The residue pigment in the reservoir was detected by absorbance spectroscopy (630 nm) in time courses. At the flow rates of 3 $\mu\text{L}/\text{min}$ and 5 $\mu\text{L}/\text{min}$, less than 5% of the blue dye remained in the reservoir after 5 min (**Fig. 4D, E**). With 10 $\mu\text{L}/\text{min}$, > 95% of the dye was washed out within 2 min (**Fig. 4F**). These results validated the efficient turnover of liquid samples in the microfluidic reservoirs.

The analytical merits of the sensor

We screen-printed Ca^{2+} selective electrodes onto the fabric-based microfluidics to validate its applicability. Ca^{2+} was chosen because this ion is an important participator of metabolism and mineral homeostasis. Unusual changes in Ca^{2+} concentrations can indicate possible diseases such as cirrhosis, renal failure, and myeloma.⁵⁵ Our ABS film printing technology can be easily scaled up for simultaneous multi-device fabrication. **Fig. 5A** shows an example of four identical patterns on an ABS film, with each microfluidic device containing three oval reservoirs connected by channels of 800 μm wide. As shown in **Fig. 5B**, the two side reservoirs had Ca^{2+} indicator electrodes while the middle one had the reference electrode. The surface of the Ca^{2+} selective electrodes is a layer of PVC premixed with the Ca^{2+} ionophore, N,N,N',N'-Tetracyclohexyl-3-oxapentanediamide, which has hydrophilic pocket that forms a binding site specific for a Ca^{2+} ,⁵³ creating a cross-membrane potential as a function of Ca^{2+} amounts. The two indicator electrodes were identical for duplicate measurements in each run. Wires were soldered onto the leads of the printed electrodes for conduction. **Fig. 5C** shows a common Arduino UNO board (top) and a miniaturized Nano board (bottom). We used the Nano board because of the small size, which is ideal for wearable applications.

We first characterized the analytical merits of the fabric-based microfluidic sensor for Ca^{2+} quantitation. The indicator electrodes were connected to the A0 and A6 port, and the reference

electrode to the GND port of the Arduino board. The board was connected to a laptop via a USB cable. A coding was developed to measure the potential differences between the indicator and reference electrodes (**Fig. S6** in the SI). Potentiometric voltages are typically in the range of tens to hundreds of mV, which can be accurately detected by Arduino without signal amplification.

Fig. 5D shows near real-time measurements of Ca^{2+} standards (in artificial sweat) of 0.125 mM to 2 mM, flown through the sensor with a pumping setup similar to **Fig. 4C**. This concentration range covers physiological Ca^{2+} content in sweat.⁵³ With increased Ca^{2+} , higher voltages were detected, in a linear Nernst way as shown in **Fig. 5E**. The limit of detection (LOD) was determined to be 5.8 μM , consistent with most published works focusing on Ca^{2+} measurements, which were in the single digit μM range.⁵⁶⁻⁶⁰ This is sufficient for wearable Ca^{2+} detection because the physiological range in sweat is mainly around 0.2 mM to 2 mM.^{52, 53} A table is available in the SI summarizing the prior works.

Selectivity can be an issue in potentiometric measurements. To validate the high selectivity towards Ca^{2+} of our sensor, we tested the common cations in large amounts in sweat, including H^+ , K^+ , Na^+ , and Mg^{2+} . As indicated in **Fig. 5F**, these ions (comparable to physiological amount) did not interfere with the Ca^{2+} sensing. To validate the accuracy of the sensor. Two Ca^{2+} standards were made by Ratajczak and given to Zhang blindly for concentration recovery. As shown in **Fig. 5G**, the detected concentrations were not significantly different from the recipe concentrations, suggesting accurate measurements by the sensor. Note that the data in **Fig. 5E** and **G** were the average of multiple (>10) microfluidic sensors. The small error bars (especially on the calibration curve) confirmed the reproducibility of the sensor system.

Apply the sensor on human surface for wireless Ca^{2+} sensing

As shown in **Fig. 6A**, the fabric-based microfluidic sensor was worn on the arm of the tester via surgical tape. The sensor was coupled to an Arduino Nano board which was placed in a 3D printed holder fastened to the arm by a sport band. Two lithium coin batteries (CR2032) of 3.3 V were included in the holder to power the system. The setup details are shown in **Fig. S4** in the SI. Specific coding was developed for data collection, recording, and wireless transfer to a cell phone, as seen in **Fig. S5** and **S6** in the SI. **Fig. 6B** illustrates near real-time wireless [Ca^{2+}] receiving on the free App of Phyphox.⁶¹ **Fig. 6C** shows the plotted results. During the 25 min monitoring, the concentration of Ca^{2+} was average between the two working electrodes every 2 min (5 s per reading, 24 readings within 2 min were averaged). The data showed a peak concentration between 10 and

15 min, followed by a gradual decrease. The red dots are ion-chromatography analyses of Ca^{2+} from sweat sampled near the worn sensor at the designated time points, which were highly consistent with our sensor results without significant differences, strongly indicating the high accuracy of our sensor system. Exercise will first induce increased electrolyte concentrations in sweat due to dehydration.^{23, 62} Then, vigorous exercise leads to parathyroid glands to release parathyroid hormone release, which stimulates bone resorption of free Ca^{2+} , and thus reduced $[\text{Ca}^{2+}]$.⁶³ These physiological facts were consistent with our quantitations by the fabric-based microfluidic sensor.

We also tested a control sensor without the microfluidic structure—only with electrodes screen-printed exactly the same way on fabric squares. As shown in **Fig. 6D**, significant discrepancies between the sensor data and the ion-chromatography data were produced. This discrepancy enlarged with time—at 10 min, a 10.5% difference was observed while at 20 min, it was 28.12%. The sensor values were significantly higher than the real concentrations (red dots, validated by ion chromatography). This was likely caused by insufficient sample refreshment at the electrode areas, where Ca^{2+} content kept accumulating. These data demonstrated the necessity to include microfluidics for efficient sample delivery in such sensors.

In addition to wearing the sensor stand-alone, we could also make the sensor a module of a T-shirt. As shown in **Fig. 7A**, a square was cut on the sleeve, which was covered by a plain fabric square when not used, via regular or hook-and-loop tape. Whenever needed, the plain fabric square was replaced by the fabric-based microfluidic device for near real-time detections (**Fig. 7B, C**) and results reading on a cell phone. We tested the scheme and found a similar trend of $[\text{Ca}^{2+}]$ in the sweat (**Fig. 7D**) as in **Fig. 6C**, with a peak between 10 and 15 min, followed by a slow decrease.

Conclusion

We developed a fabric-based microfluidic sensor platform for wearable health monitoring. A new technology using ABS film printing was contributed, which can produce precise and reproducible fabric-based microfluidics with the potential of scaled mass-production. We also creatively developed an Arduino-based potentiometer for wearable data collection, recording,

processing, and wireless transfer. The simplicity of Arduino and the open-source nature of the related software will potentially facilitate the wide adoption of wearable sensing. We validated the sensor system by measuring $[Ca^{2+}]$ in sweat in near real-time, with accurate results generated. Meanwhile, the necessity of having microfluidic features for sweat delivery was also confirmed. We applied the sensor standalone, or as a module of T-shirts, the success of which represents a critical step forward towards the ultimate goal of biochemically smart clothes.

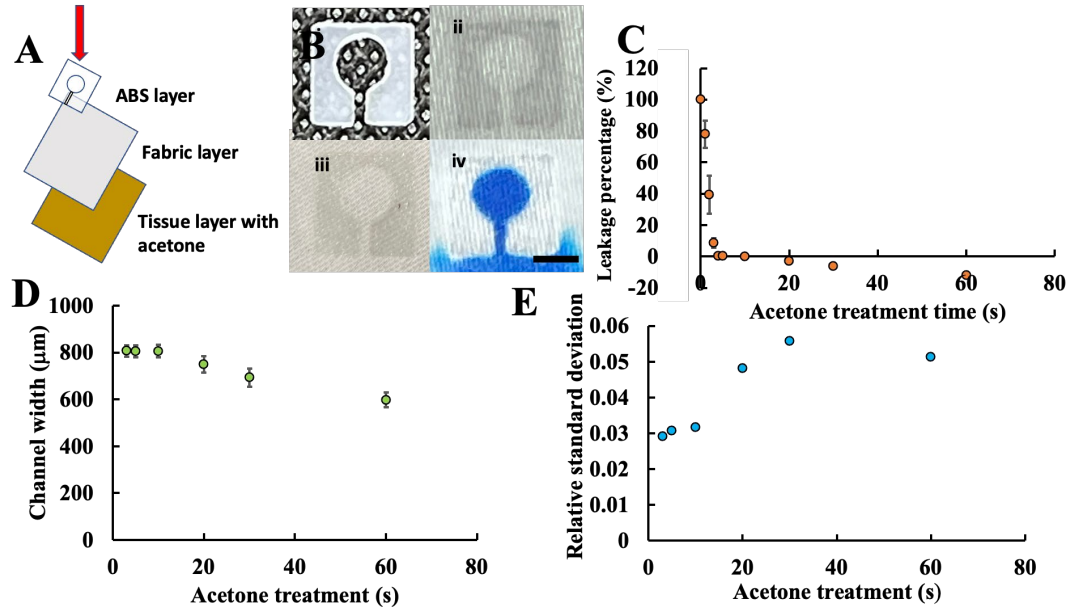


Figure 1. The new technology to make fabric-based microfluidics. **(A)** Illustration of the fabrication process. **(B)** Image of the laser-cut ABS film (i); front (ii) and back (iii) views of the resulting fabric-based microfluidic; blue dye filling the reservoir and channel (iv). (Scale bar = 5 mm). **(C)** Leakage percentage as a function of the acetone treatment time. (N=5, error bars = standard deviation). **(D)** Channel widths after the various acetone treatment times (Designed as 800 μm). (N=5, error bars= standard deviation). **(E)** Relative standard deviations of widths at different locations of the same channel after the different acetone treatment times.

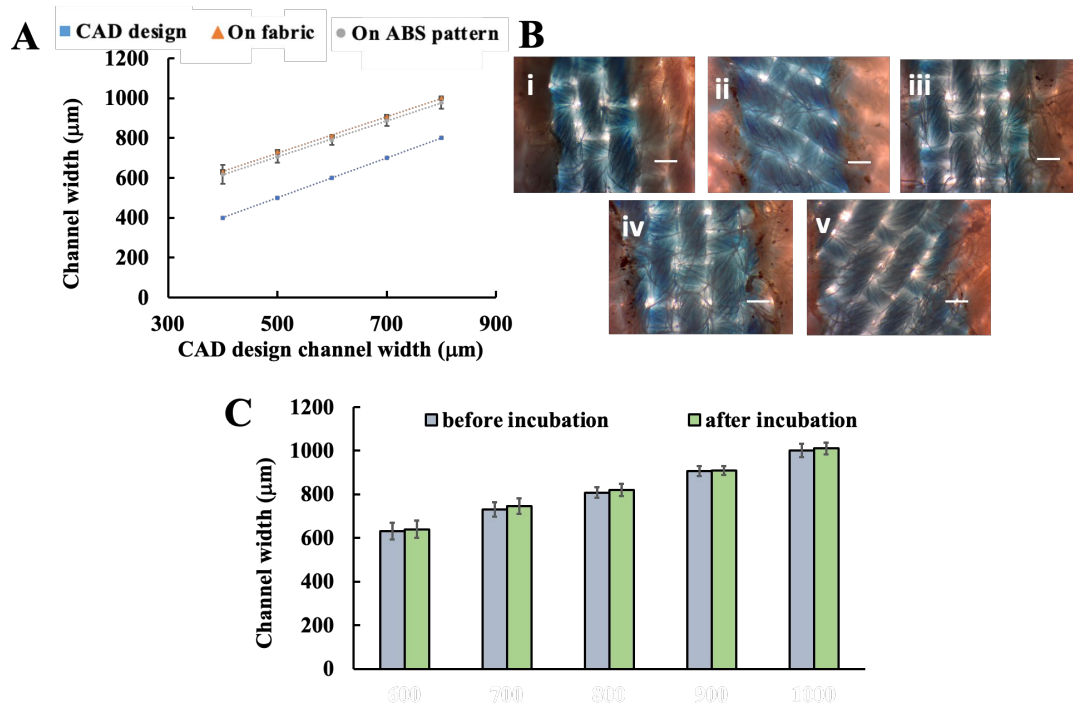


Figure 2. Characterization of fabric-based microfluidics. **(A)** The channel width in CAD design (blue), ABS pattern after laser cutting (grey), and actual microfluidics on cotton fabric (orange). (N=5, error = standard deviation). **(B)** Channels of fabric-based microfluidics from 600-1000 μm marked by a blue dye. (Scale bars = 200 μm). **(C)** The channel widths before and after 37 $^{\circ}\text{C}$ incubation. (N=5, error bar= standard deviation).

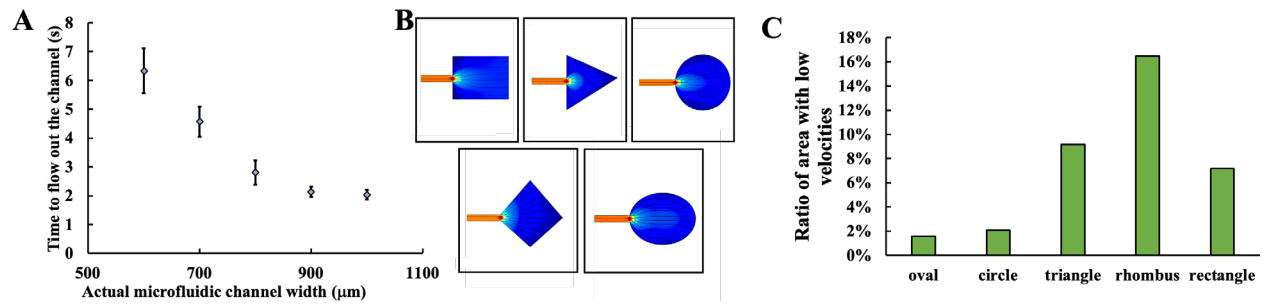


Figure 3. Experiments and simulations to determine the optimal channel size and reservoir shape. **(A)** With a larger channel width, faster drainage was observed, which then plateaued after 800 μm . (N=5, error = standard deviation). **(B)** Velocity field simulation in reservoirs of the various shapes. **(C)** Percentage of the lowest-velocity areas (<15% of gross average) in the different shapes.

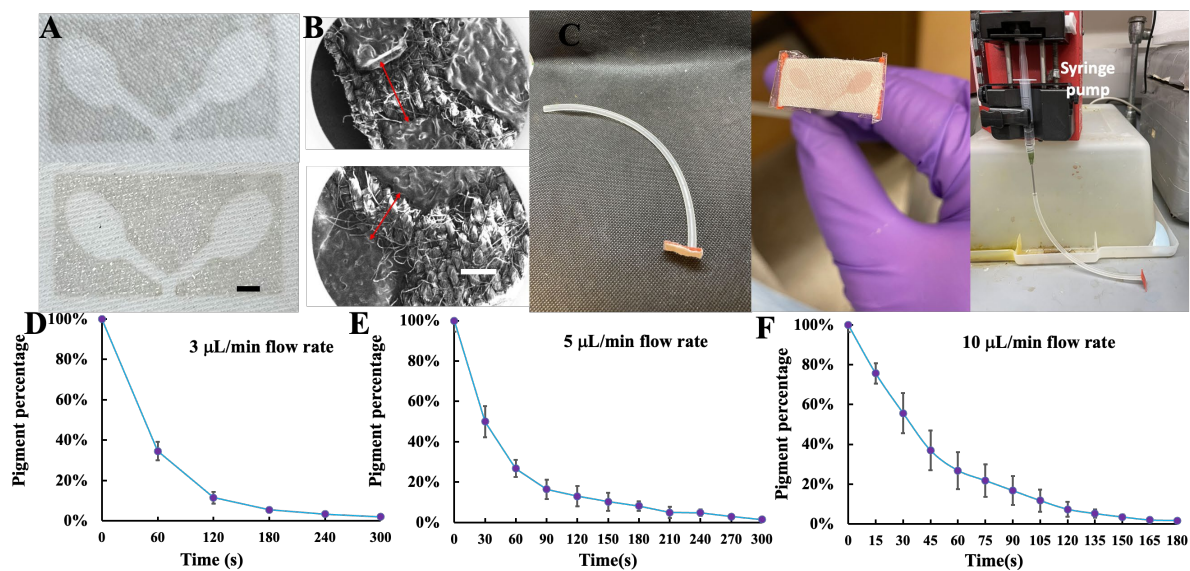


Figure 4. (A) Fabric-based microfluidics with the optimized reservoir shape and channel width. (Scale bar = 1 mm). (B) SEM views of the joint (top) and individual (bottom) channels of such a device. (Scale bar = 500 μm). (C) The setup to test the washing efficiency. (D-F) Residue dye in the reservoirs as a function of time at the various flow rates. Error bars=standard deviation.

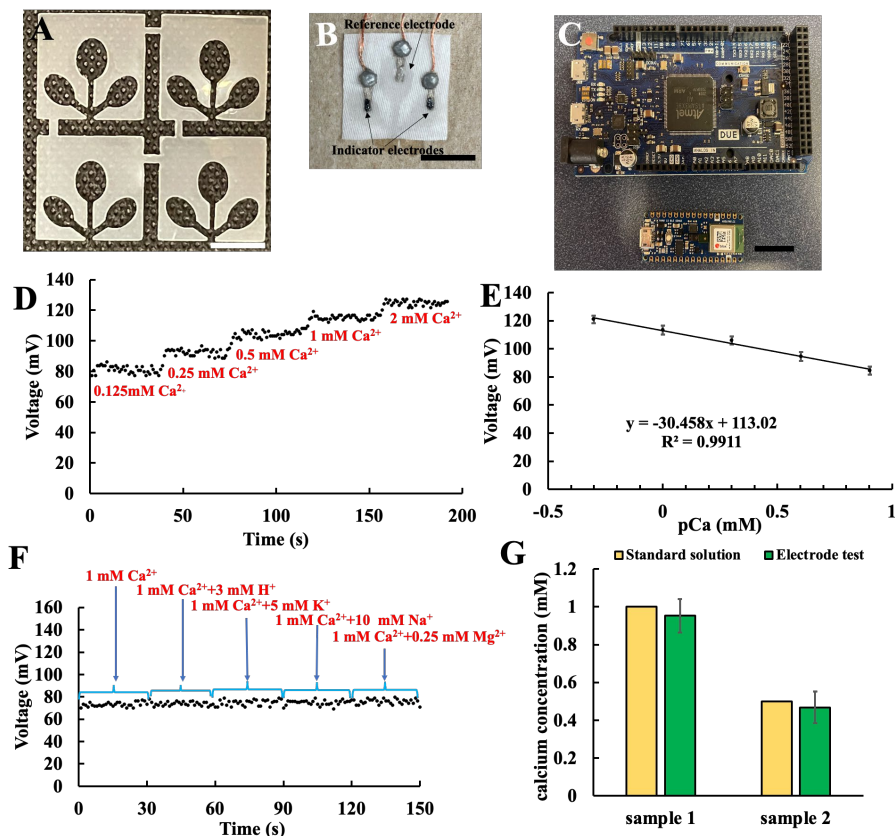


Figure 5. Analytical merit evaluation. **(A)** Laser-cut ABS patterns for simultaneous multi-device fabrication. (Scale bar = 10 mm). **(B)** Electrodes were screen-printed on the fabric-based microfluidics. The electrodes on the side reservoirs (black) were identical indicator electrodes for duplicate measurements in each experiment, and the silver electrode in the middle reservoir was the Ag/AgCl reference electrode. (Scale bar = 10 mm). **(C)** Arduino Due and Nano boards. (Scale bar = 10 mm). **(D)** Responses of Ca²⁺ standards on the sensor. **(E)** Calibration curve of Ca²⁺ responses (voltage vs. pCa). **(F)** Selectivity tests of the Ca²⁺ electrodes. **(G)** Accuracy tests of the Ca²⁺ sensor. (N=3, error bar = standard deviation).

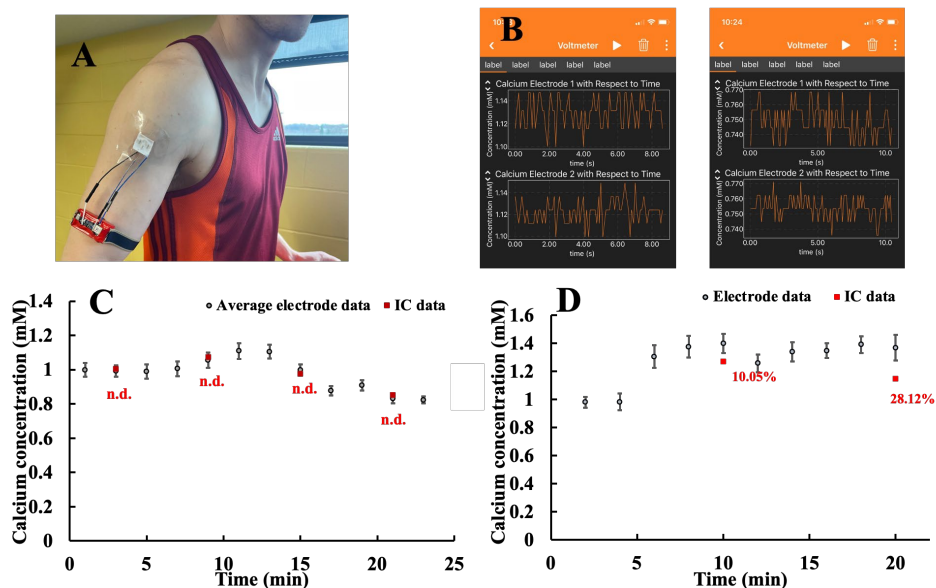


Figure 6. Ca^{2+} measurements by the wearable fabric-based microfluidic sensor. **(A)** The setup. **(B)** Near real-time wireless collection of the processed data (by the programmed Arduino) in the APP of Phyphox. **(C)** Detected calcium amounts in sweat (data within 2 min were averaged) by our two sensors (grey), and by the validation method of ion chromatography (red). (n.d.= no significant difference, error bar = standard error of mean). **(D)** Detected calcium concentrations using the same electrodes on the same fabric but without the microfluidic feature (grey). Significant discrepancies were observed from the validated data (red), indicating the necessity of microfluidics to refresh sweat in the detection zone. (Error bar = standard error of mean).

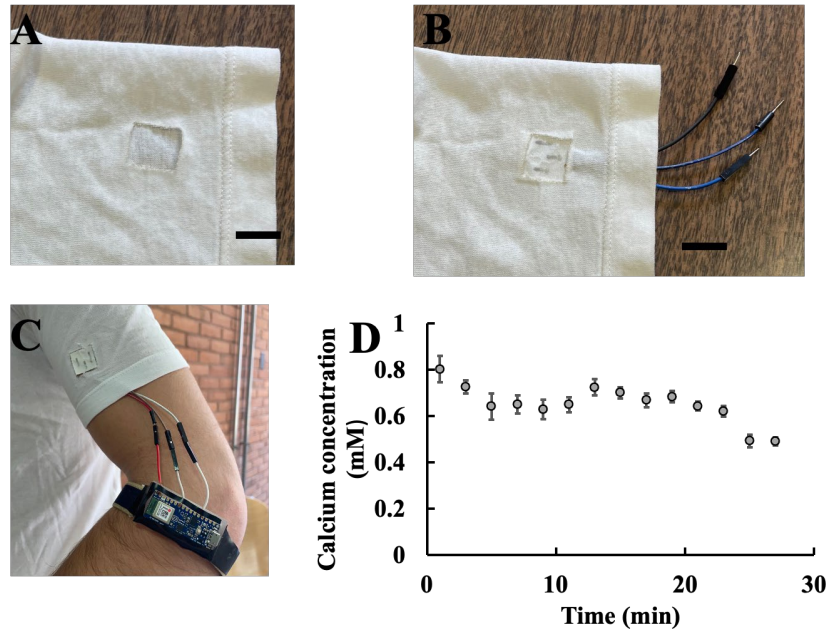
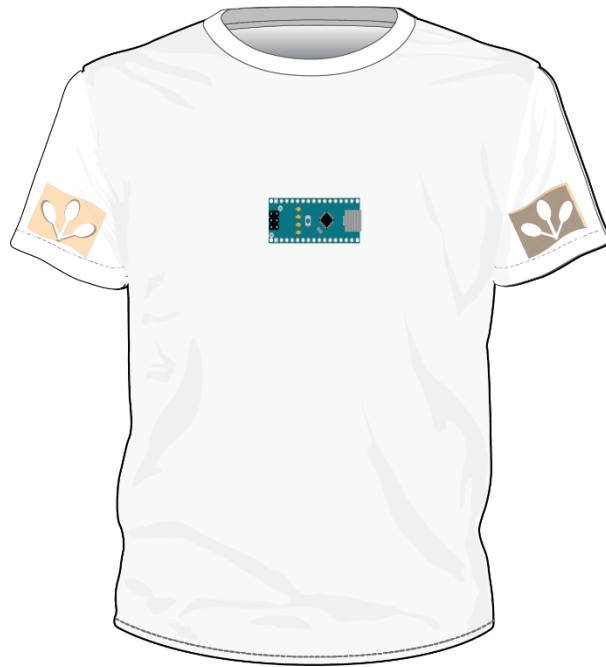


Figure 7. The fabric-based microfluidic sensor as a module of a t-shirt. **(A)** Laser cutting a spare to fit in the sensor. (Scale bar = 20 mm). **(B)** Integrating the sensor to the t-shirt. Scale bar = 20 mm. **(C)** Combining the Arduino potentiometer to the fabric-based microfluidics. **(D)** Near real-time measurements of $[Ca^{2+}]$ with the t-shirt sensor. Error bar= standard error of mean.

Supporting information

Additional experimental details, materials, and methods, including photographs of experimental setup are shown in **Fig. S1** to **S7** and **Table S1** in the supporting information.

For TOC only



REFERENCES

1. Pirovano, P.; Dorrian, M.; Shinde, A.; Donohoe, A.; Brady, A. J.; Moyna, N. M.; Wallace, G.; Diamond, D.; McCaul, M., A wearable sensor for the detection of sodium and potassium in human sweat during exercise. *Talanta* **2020**, *219*, 121145.
2. Quer, G.; Radin, J. M.; Gadaleta, M.; Baca-Motes, K.; Ariniello, L.; Ramos, E.; Kheterpal, V.; Topol, E. J.; Steinhubl, S. R., Wearable sensor data and self-reported symptoms for COVID-19 detection. *Nature Medicine* **2021**, *27* (1), 73-77.
3. Currano, L. J.; Sage, F. C.; Hagedon, M.; Hamilton, L.; Patrone, J.; Gerasopoulos, K., Wearable Sensor System for Detection of Lactate in Sweat. *Scientific Reports* **2018**, *8* (1), 15890.
4. Silva, R. R.; Raymundo-Pereira, P. A.; Campos, A. M.; Wilson, D.; Otoni, C. G.; Barud, H. S.; Costa, C. A. R.; Domenegueti, R. R.; Balogh, D. T.; Ribeiro, S. J. L.; Oliveira Jr, O. N., Microbial nanocellulose adherent to human skin used in electrochemical sensors to detect metal ions and biomarkers in sweat. *Talanta* **2020**, *218*, 121153.
5. Li, S.; Ma, Z.; Cao, Z.; Pan, L.; Shi, Y., Advanced Wearable Microfluidic Sensors for Healthcare Monitoring. *Small* **2020**, *16* (9), 1903822.
6. Zhang, T.; Monia Kabandana, G. K.; Ratajczak, A. M.; Chen, C., A quantitative sensing system based on a 3D-printed ion-selective electrode for rapid and sensitive detection of bacteria in biological fluid. *Talanta* **2022**, *238*, 123040.
7. Xu, T.; Peng, F.; Zhang, T.; Chi, B.; Xu, H.; Mao, C.; Feng, S., Poly(γ -glutamic acid), coagulation? Anticoagulation? *Journal of Biomaterials Science, Polymer Edition* **2016**, *27* (16), 1599-1610.
8. Ashton, N. J.; Hye, A.; Rajkumar, A. P.; Leuzy, A.; Snowden, S.; Suárez-Calvet, M.; Karikari, T. K.; Schöll, M.; La Joie, R.; Rabinovici, G. D.; Höglund, K.; Ballard, C.; Hortobágyi, T.; Svenningsson, P.; Blennow, K.; Zetterberg, H.; Aarsland, D., An update on blood-based biomarkers for non-Alzheimer neurodegenerative disorders. *Nature Reviews Neurology* **2020**, *16* (5), 265-284.
9. You, J.; Willcox, M. D.; Madigan, M. C.; Wasinger, V.; Schiller, B.; Walsh, B. J.; Graham, P. H.; Kearsley, J. H.; Li, Y., Chapter Four - Tear Fluid Protein Biomarkers. In *Advances in Clinical Chemistry*, Makowski, G. S., Ed. Elsevier: 2013; Vol. 62, pp 151-196.
10. Gadalla, A. A. H.; Friberg, I. M.; Kift-Morgan, A.; Zhang, J.; Eberl, M.; Topley, N.; Weeks, I.; Cuff, S.; Wootton, M.; Gal, M.; Parekh, G.; Davis, P.; Gregory, C.; Hood, K.; Hughes, K.; Butler, C.; Francis, N. A., Identification of clinical and urine biomarkers for uncomplicated urinary tract infection using machine learning algorithms. *Scientific Reports* **2019**, *9* (1), 19694.
11. Bandodkar, A. J.; Wang, J., Non-invasive wearable electrochemical sensors: a review. *Trends in Biotechnology* **2014**, *32* (7), 363-371.
12. Ghaffari, R.; Rogers, J. A.; Ray, T. R., Recent progress, challenges, and opportunities for wearable biochemical sensors for sweat analysis. *Sensors and Actuators B: Chemical* **2021**, *332*, 129447.
13. Xiao, J.; Fan, C.; Xu, T.; Su, L.; Zhang, X., An electrochemical wearable sensor for levodopa quantification in sweat based on a metal–Organic framework/graphene oxide composite with integrated enzymes. *Sensors and Actuators B: Chemical* **2022**, *359*, 131586.

14. Moonen, E. J. M.; Haakma, J. R.; Peri, E.; Pelssers, E.; Mischi, M.; den Toonder, J. M. J., Wearable sweat sensing for prolonged, semicontinuous, and nonobtrusive health monitoring. *VIEW* **2020**, *1* (4), 20200077.
15. Yang, P.; Wei, G.; Liu, A.; Huo, F.; Zhang, Z., A review of sampling, energy supply and intelligent monitoring for long-term sweat sensors. *npj Flexible Electronics* **2022**, *6* (1), 33.
16. Brueck, A.; Iftekhar, T.; Stannard, A. B.; Yelamarthi, K.; Kaya, T., A Real-Time Wireless Sweat Rate Measurement System for Physical Activity Monitoring. *Sensors (Basel)* **2018**, *18* (2).
17. Emaminejad, S.; Gao, W.; Wu, E.; Davies, Z. A.; Yin Yin Nyein, H.; Challa, S.; Ryan, S. P.; Fahad, H. M.; Chen, K.; Shahpar, Z.; Talebi, S.; Milla, C.; Javey, A.; Davis, R. W., Autonomous sweat extraction and analysis applied to cystic fibrosis and glucose monitoring using a fully integrated wearable platform. *Proceedings of the National Academy of Sciences* **2017**, *114* (18), 4625-4630.
18. Anastasova, S.; Crewther, B.; Bembnowicz, P.; Curto, V.; Ip, H. M. D.; Rosa, B.; Yang, G.-Z., A wearable multisensing patch for continuous sweat monitoring. *Biosensors and Bioelectronics* **2017**, *93*, 139-145.
19. Sim, D.; Brothers, M. C.; Slocik, J. M.; Islam, A. E.; Maruyama, B.; Grigsby, C. C.; Naik, R. R.; Kim, S. S., Biomarkers and Detection Platforms for Human Health and Performance Monitoring: A Review. *Advanced Science* **2022**, *9* (7), 2104426.
20. Wang, Z.; Shin, J.; Park, J.-H.; Lee, H.; Kim, D.-H.; Liu, H., Engineering Materials for Electrochemical Sweat Sensing. *Advanced Functional Materials* **2021**, *31* (12), 2008130.
21. Sempionatto, J. R.; Moon, J.-M.; Wang, J., Touch-Based Fingertip Blood-Free Reliable Glucose Monitoring: Personalized Data Processing for Predicting Blood Glucose Concentrations. *ACS Sens.* **2021**, *6* (5), 1875-1883.
22. Koh, A.; Kang, D.; Xue, Y.; Lee, S.; Pielak, R. M.; Kim, J.; Hwang, T.; Min, S.; Banks, A.; Bastien, P.; Manco, M. C.; Wang, L.; Ammann, K. R.; Jang, K.-I.; Won, P.; Han, S.; Ghaffari, R.; Paik, U.; Slepian, M. J.; Balooch, G.; Huang, Y.; Rogers, J. A., A soft, wearable microfluidic device for the capture, storage, and colorimetric sensing of sweat. *Science Translational Medicine* **2016**, *8* (366), 366ra165-366ra165.
23. Gao, W.; Emaminejad, S.; Nyein, H. Y. Y.; Challa, S.; Chen, K.; Peck, A.; Fahad, H. M.; Ota, H.; Shiraki, H.; Kiriya, D.; Lien, D.-H.; Brooks, G. A.; Davis, R. W.; Javey, A., Fully integrated wearable sensor arrays for multiplexed in situ perspiration analysis. *Nature* **2016**, *529* (7587), 509-514.
24. Wang, Y.; Wang, X.; Lu, W.; Yuan, Q.; Zheng, Y.; Yao, B., A thin film polyethylene terephthalate (PET) electrochemical sensor for detection of glucose in sweat. *Talanta* **2019**, *198*, 86-92.
25. Zhang, J.; Song, R.; Zhao, X.; Fang, R.; Zhang, B.; Qian, W.; Zhang, J.; Liu, C.; He, D., Flexible Graphene-Assembled Film-Based Antenna for Wireless Wearable Sensor with Miniaturized Size and High Sensitivity. *ACS Omega* **2020**, *5* (22), 12937-12943.
26. Bariya, M.; Nyein, H. Y. Y.; Javey, A., Wearable sweat sensors. *Nature Electronics* **2018**, *1* (3), 160-171.
27. Raj M, K.; Chakraborty, S., PDMS microfluidics: A mini review. *Journal of Applied Polymer Science* **2020**, *137* (27), 48958.
28. Akther, F.; Yakob, S. B.; Nguyen, N.-T.; Ta, H. T., Surface Modification Techniques for Endothelial Cell Seeding in PDMS Microfluidic Devices. *Biosensors* **2020**, *10* (11), 182.

29. de Almeida Monteiro Melo Ferraz, M.; Nagashima, J. B.; Venzac, B.; Le Gac, S.; Songsasen, N., 3D printed mold leachates in PDMS microfluidic devices. *Scientific Reports* **2020**, *10* (1), 994.
30. Morbioli, G. G.; Speller, N. C.; Stockton, A. M., A practical guide to rapid-prototyping of PDMS-based microfluidic devices: A tutorial. *Analytica Chimica Acta* **2020**, *1135*, 150-174.
31. Martinez, A. W.; Phillips, S. T.; Whitesides, G. M., Three-dimensional microfluidic devices fabricated in layered paper and tape. *Proceedings of the National Academy of Sciences* **2008**, *105* (50), 19606-19611.
32. Martinez, A. W.; Phillips, S. T.; Whitesides, G. M.; Carrilho, E., Diagnostics for the Developing World: Microfluidic Paper-Based Analytical Devices. *Analytical Chemistry* **2010**, *82* (1), 3-10.
33. Dungchai, W.; Chailapakul, O.; Henry, C. S., Electrochemical Detection for Paper-Based Microfluidics. *Analytical Chemistry* **2009**, *81* (14), 5821-5826.
34. Cincotto, F. H.; Fava, E. L.; Moraes, F. C.; Fatibello-Filho, O.; Faria, R. C., A new disposable microfluidic electrochemical paper-based device for the simultaneous determination of clinical biomarkers. *Talanta* **2019**, *195*, 62-68.
35. Liu, J.; Kong, X.; Wang, H.; Zhang, Y.; Fan, Y., Roll-to-roll wax transfer for rapid and batch fabrication of paper-based microfluidics. *Microfluidics and Nanofluidics* **2019**, *24* (1), 6.
36. Liu, P.; Li, B.; Fu, L.; Huang, Y.; Man, M.; Qi, J.; Sun, X.; Kang, Q.; Shen, D.; Chen, L., Hybrid Three Dimensionally Printed Paper-Based Microfluidic Platform for Investigating a Cell's Apoptosis and Intracellular Cross-Talk. *ACS Sens.* **2020**, *5* (2), 464-473.
37. Altundemir, S.; Uguz, A. K.; Ulgen, K., A review on wax printed microfluidic paper-based devices for international health. *Biomicrofluidics* **2017**, *11* (4), 041501.
38. Dungchai, W.; Chailapakul, O.; Henry, C. S., A low-cost, simple, and rapid fabrication method for paper-based microfluidics using wax screen-printing. *Analyst* **2011**, *136* (1), 77-82.
39. Nilghaz, A.; Liu, X.; Ma, L.; Huang, Q.; Lu, X., Development of fabric-based microfluidic devices by wax printing. *Cellulose* **2019**, *26* (5), 3589-3599.
40. Tang, K.-P. M.; Kan, C.-W.; Fan, J.-t., Evaluation of water absorption and transport property of fabrics. *Textile Progress* **2014**, *46* (1), 1-132.
41. Liu, M.; Zhang, C.; Liu, F., Understanding wax screen-printing: A novel patterning process for microfluidic cloth-based analytical devices. *Analytica Chimica Acta* **2015**, *891*, 234-246.
42. Vatansever, F.; Burtovyy, R.; Zdyrko, B.; Ramaratnam, K.; Andrukh, T.; Minko, S.; Owens, J. R.; Kornev, K. G.; Luzinov, I., Toward Fabric-Based Flexible Microfluidic Devices: Pointed Surface Modification for pH Sensitive Liquid Transport. *ACS Applied Materials & Interfaces* **2012**, *4* (9), 4541-4548.
43. Farajikhah, S.; Cabot, J. M.; Innis, P. C.; Paull, B.; Wallace, G., Life-Saving Threads: Advances in Textile-Based Analytical Devices. *ACS Combinatorial Science* **2019**, *21* (4), 229-240.
44. Prabhu, A.; Giri Nandagopal, M. S.; Peralam Yegneswaran, P.; Singhal, H. R.; Mani, N. K., Inkjet printing of paraffin on paper allows low-cost point-of-care diagnostics for pathogenic fungi. *Cellulose* **2020**, *27* (13), 7691-7701.
45. Rantamäki, A. H.; Wiedmer, S. K.; Holopainen, J. M., Melting Points—The Key to the Anti-Evaporative Effect of the Tear Film Wax Esters. *Investigative Ophthalmology & Visual Science* **2013**, *54* (8), 5211-5217.

46. Lim, C. L.; Byrne, C.; Lee, J. K., Human thermoregulation and measurement of body temperature in exercise and clinical settings. *Annals Academy of Medicine Singapore* **2008**, *37* (4), 347.
47. Urbanski, J. P.; Thies, W.; Rhodes, C.; Amarasinghe, S.; Thorsen, T., Digital microfluidics using soft lithography. *Lab on a Chip* **2006**, *6* (1), 96-104.
48. Carrilho, E.; Phillips, S. T.; Vella, S. J.; Martinez, A. W.; Whitesides, G. M., Paper Microzone Plates. *Analytical Chemistry* **2009**, *81* (15), 5990-5998.
49. Zhang, Y.; Duan, H.; Li, G.; Peng, M.; Ma, X.; Li, M.; Yan, S., Construction of liquid metal-based soft microfluidic sensors via soft lithography. *Journal of Nanobiotechnology* **2022**, *20* (1), 246.
50. Lee, M. H.; Huntington, M. D.; Zhou, W.; Yang, J.-C.; Odom, T. W., Programmable Soft Lithography: Solvent-Assisted Nanoscale Embossing. *Nano Letters* **2011**, *11* (2), 311-315.
51. Abidi, N.; Cabrales, L.; Hequet, E., Functionalization of a Cotton Fabric Surface with Titania Nanosols: Applications for Self-Cleaning and UV-Protection Properties. *ACS Applied Materials & Interfaces* **2009**, *1* (10), 2141-2146.
52. Parrilla, M.; Cuartero, M.; Crespo, G. A., Wearable potentiometric ion sensors. *TrAC Trends in Analytical Chemistry* **2019**, *110*, 303-320.
53. Nyein, H. Y. Y.; Gao, W.; Shahpar, Z.; Emaminejad, S.; Challa, S.; Chen, K.; Fahad, H. M.; Tai, L.-C.; Ota, H.; Davis, R. W.; Javey, A., A Wearable Electrochemical Platform for Noninvasive Simultaneous Monitoring of Ca²⁺ and pH. *ACS Nano* **2016**, *10* (7), 7216-7224.
54. Vajdi, M.; Moghanlou, F. S.; Sharifianjazi, F.; Asl, M. S.; Shokouhimehr, M., A review on the Comsol Multiphysics studies of heat transfer in advanced ceramics. *Journal of Composites and Compounds* **2020**, *2* (2), 35-43.
55. Robertson, W. G.; Marshall, R. W., Ionized calcium in body fluids. *Crit Rev Clin Lab Sci* **1981**, *15* (2), 85-125.
56. Park, S.; Maier, C. S.; Koley, D., Anodic stripping voltammetry on a carbon-based ion-selective electrode. *Electrochim. Acta* **2021**, *390*, 138855.
57. Keene, S. T.; Fogarty, D.; Cooke, R.; Casadevall, C. D.; Salleo, A.; Parlak, O., Wearable Organic Electrochemical Transistor Patch for Multiplexed Sensing of Calcium and Ammonium Ions from Human Perspiration. *Advanced Healthcare Materials* **2019**, *8* (24), 1901321.
58. Lee, Y. K.; Jang, K.-I.; Ma, Y.; Koh, A.; Chen, H.; Jung, H. N.; Kim, Y.; Kwak, J. W.; Wang, L.; Xue, Y.; Yang, Y.; Tian, W.; Jiang, Y.; Zhang, Y.; Feng, X.; Huang, Y.; Rogers, J. A., Chemical Sensing Systems that Utilize Soft Electronics on Thin Elastomeric Substrates with Open Cellular Designs. *Advanced Functional Materials* **2017**, *27* (9), 1605476.
59. Kim, T.; Yi, Q.; Hoang, E.; Esfandyarpour, R., A 3D Printed Wearable Bioelectronic Patch for Multi-Sensing and In Situ Sweat Electrolyte Monitoring. *Advanced Materials Technologies* **2021**, *6* (4), 2001021.
60. Coppedè, N.; Giannetto, M.; Villani, M.; Lucchini, V.; Battista, E.; Careri, M.; Zappettini, A., Ion selective textile organic electrochemical transistor for wearable sweat monitoring. *Organic Electronics* **2020**, *78*, 105579.
61. Staacks, S.; Hütz, S.; Heinke, H.; Stampfer, C., Advanced tools for smartphone-based experiments: phyphox. *Physics Education* **2018**, *53* (4), 045009.

62. Morgan, R.; Patterson, M.; Nimmo, M., Acute effects of dehydration on sweat composition in men during prolonged exercise in the heat. *Acta Physiologica Scandinavica* **2004**, *182* (1), 37-43.
63. Kohrt, W. M.; Wherry, S. J.; Wolfe, P.; Sherk, V. D.; Wellington, T.; Swanson, C. M.; Weaver, C. M.; Boxer, R. S., Maintenance of Serum Ionized Calcium During Exercise Attenuates Parathyroid Hormone and Bone Resorption Responses. *J Bone Miner Res* **2018**, *33* (7), 1326-1334.